Article

Acoplanarity, Aromaticity, Chirality, and Helical Twisting Power of Chlorin e6 13(N)-Methylamide-15,17-dimethyl Ester Complexes: Effect of a Metal

Vladimir Burmistrov *, Viktor Aleksandriiskii *, Igor Novikov, Alena Batrakova, Dmitry Belykh, Olga Startseva [ID]
and Oskar I. Koifman

Research Institute of Macroheterocycles of Ivanovo State University of Chemistry and Technology, Sheremetev Av. 7, 153000 Ivanovo, Russia

* Correspondence: burmistrov@isuct.ru (V.B.); nmr@isuct.ru (V.A.)

Abstract: The experimental and theoretical study of the influence of metal complexing on geometry, aromaticity, chirality, and the ability to twist the nematic phase by complexes based on modified natural chlorin e6 was carried out. The geometry optimization of the chlorin e6 13(N)-methylamide-15,17-dimethyl ester (MADMECl) and its Zn, Cu, and Ni complexes by DFT (CAM-B3LYP/6–31 G(d,p) functional) method was performed. Based on these calculations, the acoplanarity degree of the macrocyclic ligand and the distortion energy of its dianion were estimated, which allowed the arrangement of the MADMECl complexes in the series Ni > Cu > Zn. Aromaticity was evaluated using the NICS criterion (nuclear independent chemical shift). An increase in the degree of aromaticity of the macrocycle upon complex formation was established. At the same time, the aromaticity of the inner conjugation contour corresponds to the same series as the acoplanarity, while the outer π-delocalization is characterized by the reverse sequence. An experimental evaluation of the electron circular dichroism of the Soret and the Q-bands, as well as the g-factor of dissymmetry, was carried out. The growth of these parameters with an increase in the degree of acoplanarity and aromaticity of the internal conjugation contour was determined. The induction of helical phases in mixtures of nematic liquid crystals (LCs) based on cyanobiphenyls and MADMECl macrocyclic metal complexes was studied by polarization microscopy, and the clearance temperatures and helix pitch of the mesophases were measured. A strong effect of the metal on the phase transition temperature and helical twisting power was established.

Keywords: macroheterocyclic metal complexes; geometry; aromaticity; chirality; induction of helical phases; helical twisting power

1. Introduction

Macroheterocycles and their metal complexes, such as heme, chlorophyll, cyanocobalamin, etc., play an outstanding role in biological systems [1]. Chemical modification of natural macroheterocycles allows us to obtain valuable pharmacological preparations for photodynamic therapy of oncological diseases [2], disinfection of pathogenic viruses [3], and other purposes. Synthetic porphyrins, phthalocyanines, and their complexes are effective dyes, pigments [4], catalysts [5], and chromatographic stationary phases [6]. Reduced nickel porphyrins play an important role as enzymatic cofactors in the global carbon cycle (cofactor F430) and as powerful catalysts in solar-to-fuel processes [7]. The combination of Zn porphyrin dyes and copper-based electrolytes represents a sustainable route for economic and environmentally friendly dye-sensitized solar cells [8]. Axial complexes of zinc porphyrins exhibit second-order nonlinear optical properties [9]. Coordination-induced spin state switching with nickel chlorin and nickel isobacteriochlorin [10] is of undoubted interest.

A special place among macroheterocyclic metal complexes is occupied by chiral inducers of helical liquid crystalline phases [6,11]. The most notable areas of technical application of helical phases induced by chiral dopants in nonchiral LCs are electro–optical devices [12] and light-controlled liquid crystal materials [13,14]. The latter are a new generation of multifunctional supramolecular materials, the so-called smart soft materials formed by incorporating photochromic chiral dopants. They can form the basis for the application of intelligent photocontrolled liquid crystal materials in photonics, color filters, polarizers, all-optical reflective displays, laser beam control, holographic optical data storage, sensors, soft actuators, nanotechnology, etc. [13–15]. The LC-induced phases are promising for the development of chromatographic stationary phases with high chiral selectivity [16]. Based on them, flexible magnets [17], light-sensitive nanostructures [18], chiro-optical molecular switches [19–21], microlenses for biomimetic optical systems [22], highly sensitive sensors for detecting gases [23], and molecular motors [24,25] are being developed.

Chiral metal complexes are promising dopants for LCs [26–30]. Interest in them is due to the possibility of strong coordination interactions, complex dopant–LC. It should be noted that the bis-chelate imino-alkoxytitanium complex [30] exhibits helical twisting power (HTP) value of 740 μm^{-1} in MBBA, apparently one of the highest. Metal complexes with chiral ligands or the chirality of the coordination center itself were shown to exhibit a high tendency to induce helical phases. In any case, high HTP values are demonstrated by complexes with bulky planar aromatic ligands which provide rigid contact with mesogenic molecules and, hence, high efficiency of chiral transfer. Among chiral complex dopants, the metal complexes of macroheterocycles–porphyrins, phthalocyanines, and their analogues, which represent an extensive class of promising compounds, are of interest [11]. Macroheterocycles and their complexes upon LC doping can play the role not only of inducers of helical mesophases, but also stabilizers and dichroic dyes [31].

In [32], a chiral octa substituted nickel tetraporphyrinate was synthesized and tested as a dopant in nematic mixtures based on highly polar cyanobiphenyls and weakly polar Schiff bases. A high twisting energy was shown (126.5 μm^{-1} in the first case and 63.5 μm^{-1} in the second). On the basis of quantum chemical calculations and two-dimensional NMR, it was shown that the reason for the high efficiency of this dopant is a special mechanism of self-assembly in this system, which consists in axial coordination and the inclusion of LC molecules in the chiral shell of the dopant. These data allow us to conclude that macrocyclic metal complexes are promising not only as inducers of helical LC phases, but also as chemosensors based on them.

The design of chemosensors that function by reversible binding of the substrate with a chiral dopant inducer is one of the perspective directions in the field of creating smart liquid crystal materials based on induced helical mesophases. This process is accompanied by a significant change in the helix pitch and optical properties of the LC composition, fixed by various spectral methods [23,33]. The high sensitivity as receptor-dopant is demonstrated by tripodal tetradentate ligands. Their ability to twist the mesophase of the nematic LC increases dramatically when complexed with metal ions [34].

Among such objects, chiral dopants based on natural macroheterocycles and their metal complexes are very promising, due to their high optical activity, enantiomeric purity, and wide possibilities of chemical modification. For example, 13(N)-methylamide-15,17-dimethyl ether chlorin e6 (MADMECl) and its nickel complex (Ni-MADMECl) were studied in [35] as inducers of chiral nematic phases based on various LCs. The metalation of the macroheterocycle was established to result in a multiple increase in helical twisting power with respect to LCs of a different nature and polarity. Quantum chemical calculations showed that the higher twisting ability of the nickel complex of the chlorin e6 derivative is associated with a higher energy of its interaction with the LC solvent molecules. By analyzing the energy parameters of dopants solvation, it was found that this process leads to a significant distortion of their structure, especially in the case of a metal complex, which indicates a possible increase in optical activity and, as a result, the contribution of supramolecular chirality to the process of helical LC phases induction.

Taking into account such a strong influence of the metal ion on the mechanism and efficiency of chiral induction of helical LC phases, it is of undoubted interest to reveal the role of the nature of the complexing metal on the molecular parameters of chlorin e6 derivative complexes and the chirality transfer of the third level optically active dopant–nematic LC [36]. In this regard, the aim of this work was to study the structure, aromaticity, chirality, and efficiency of chiral transport of Zn, Cu, and Ni complexes with chlorin e6 13(N)-methylamide-15,17-dimethyl ester (Scheme 1).
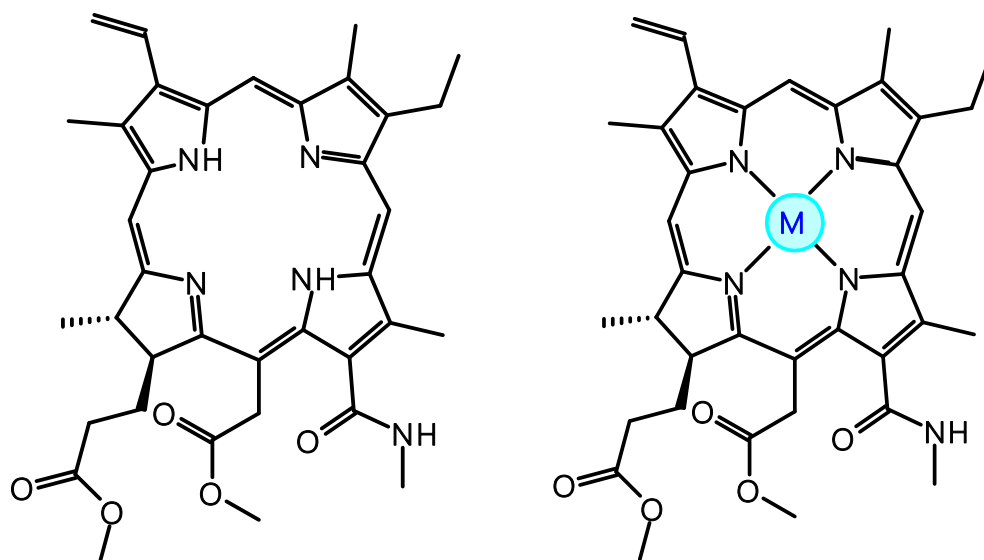
Scheme 1. MADMECl M-MADMECl (M = Zn, Cu, Ni).

2. Results and Discussion

The most objective method for assessing the configuration and optical activity of chiral substances is circular dichroism (CD) spectroscopy [37]. The configuration of the experimental visible and ECD spectra of chlorin e6 13(N)-methylamide-15,17-dimethyl ester (MADMECl), including the signs of the CD bands (Figure 1), is similar to those shown in [38] for the spectra of metal free chlorin e6 di- and trimethyl ether. Moreover, Figure 1 indicates a significant effect of the complexing metal on the chirality of macroheterocyclic complexes.

In this case, the characteristic two-band UV/Vis spectra (the Soret band and the Q-band [1]) differ insignificantly (Figure 1). Taking into account the presence of various substituents and one saturated five-membered ring in the structure of the macrocyclic ligand, as well as its asymmetry [39,40], both experimental studies and quantum chemical simulation of the structure of the metal complexes are required to elucidate the reasons for the strong influence of the metal nature on CD. The latter was carried out by the DFT method (CAM-B3LYP/6–31 G(d,p)) (see the experimental section). At the same time, due to the complexity of the macrocyclic core structure, the assessment of the simulation adequacy is of particular relevance. Therefore, based on the optimized structures of the metal complexes, the theoretical UV/Vis and ECD spectra are presented in Figure 1, and ^{1}H, ^{13}C NMR,[15]N in Supplementary Figures S1–S3, Tables S1–S3. An analysis of these data indicates a satisfactory agreement with the experimental spectral data and, therefore, the adequacy of quantum chemical calculations and the possibility of their use in assessing the chirality transfer of the second level (from the stereogenic center to the molecule of the complex [41]) and the third level (from the molecule of the complex dopant to the liquid crystal matrix) [25,26].
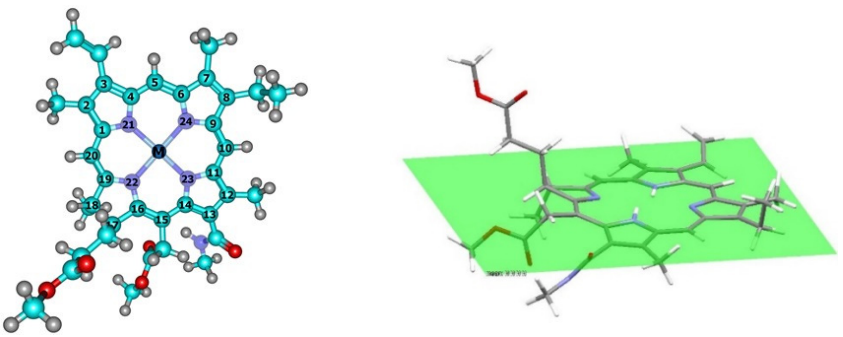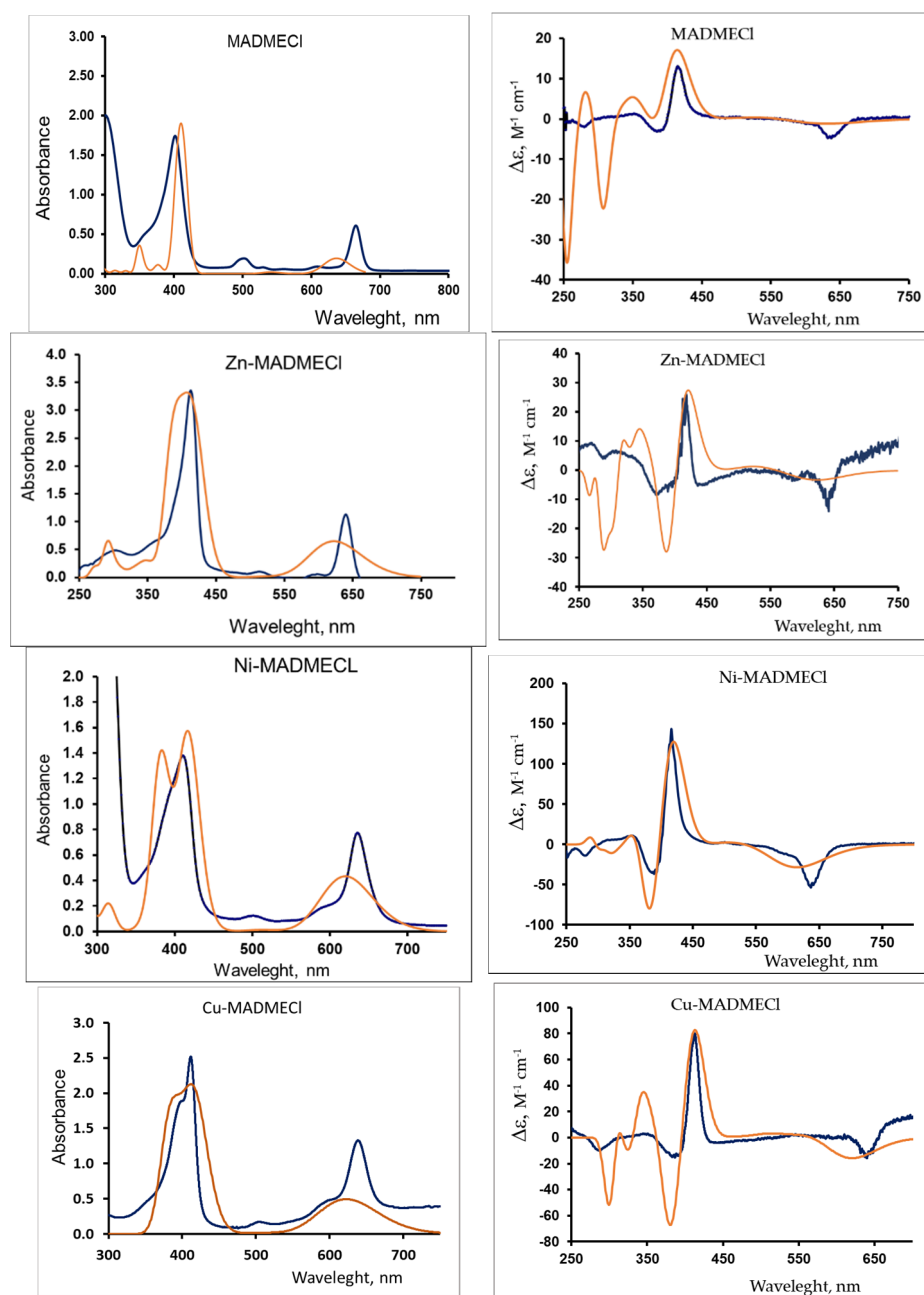
Figure 1. UV/Vis spectra (**left**) and CD spectra (**right**). Blue—experimental (chloroform, $C_{MADMECl}$ = $1.5 \cdot 10^{-4}$ M, $C_{Zn\text{-}MADMECl}$ = $3.2 \cdot 10^{-5}$ M, $C_{Cu\text{-}MADMECl}$ = $1.3 \cdot 10^{-4}$ M, $C_{Ni\text{-}MADMECl}$ = $1.1 \cdot 10^{-4}$ M); orange—calculated (TDDFT PCM-chloroform, n = 25).

A feature of chlorophyll derivatives (chlorin, pheophorbide, etc.) is the acoplanar macrocyclic core [40,42,43], which affects the properties of both ligands and metal complexes based on them.

To assess the degree of macrocycles acoplanarity on the basis of quantum chemical calculations, the distances of carbon atoms 1–20 deviations relative to the plane in which intracyclic nitrogen atoms 21–24 are located were measured (Table 1). These data indicate a greater exit of C5, C10, and C15 meso-atoms from the N4 plane compared to the carbons of the A, B, C pyrrolenine cycles (Table 1). The saturated five-membered cycle D has the highest acoplanarity. Considering the entire array of data in Table 1, we can conclude that the metal-free MADMECl has the flattest macrocycle structure. To obtain an integrated criterion for the acoplanarity of each dopant, the root mean square values of the atoms' deviation from the NNNN plane were calculated and listed in Table 1. The introduction

of the metal is accompanied by its distortion, the degree of which decreases in the series: Ni-MADMECl > Cu-MADMECl > Zn-MADMECl.

Table 1. Distances from individual atoms (Ri, Å) to the averaged NNNN plane according to CAM-B3LYP/6–31 g(d,p) data.

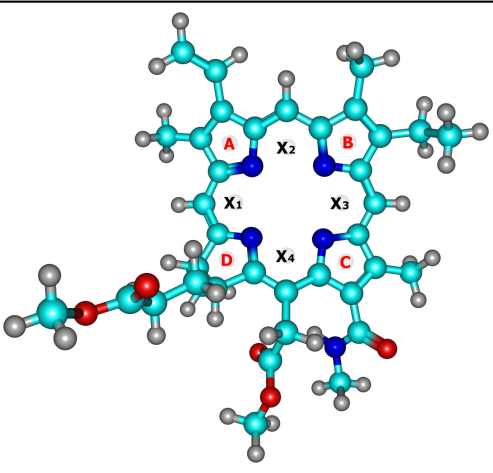| i	MADMECl	Ni-MADMECl	Zn-MADMECl	Cu-MADMECl
1	0.107	−0.426	−0.145	−0.253
2	−0.122	−0.401	−0.185	−0.293
3	0.036	0.061	0.092	−0.084
4	0.007	0.234	0.020	0.038
5	0.089	0.546	0.0931	0.231
6	0.100	0.417	0.128	0.236
7	−0.144	0.431	0.182	0.303
8	0.088	0.018	0.120	0.137
9	0.020	−0.188	0.039	0.004
10	0.084	−0.531	0.098	−0.226
11	−0.142	−0.476	−0.180	−0.293
12	−0.312	−0.598	−0.369	−0.491
13	−0.322	−0.226	−0.374	−0.382
14	0.104	0.126	0.122	−0.069
15	−0.126	0.645	0.160	0.318
16	−0.216	0.580	0.266	0.388
17	0.549	0.935	0.631	0.770
18	0.052	0.123	0.027	0.030
19	0.040	−0.271	0.036	−0.099
20	−0.131	−0.617	−0.156	−0.307
21	0.037	0.070	0.06	−0.075
22	0.037	0.069	0.06	0.076
23	0.036	0.068	0.06	−0.076
24	0.037	0.069	0.06	0.075
	H21 0.027	(Ni 0.004)	(Zn 0.016)	(Cu 0.01)
	H23 0.114			
$\sqrt{\frac{1}{n}\sum\limits_{i=1}^{N}|\Delta r_i|^2}$	0.171	0.415	0.205	0.280

This conclusion is confirmed by the analysis of nitrogen–nitrogen distances in the structures under study (Table 2). Thus, complex formation with metals, as a rule, leads to the convergence of intracyclic nitrogen atoms (when the Zn complex is formed, these changes are insignificant), and the degree of convergence is symbatic with the degree of acoplanarity: Ni-MADMECl > Cu-MADMECl > Zn-MADMECl.

Table 2. Distances between nitrogen atoms within the macrocycle according to CAM-B3LYP/6–31 g(d,p) data (designations in the previous table).

	r_{21-22}, Å	r_{22-23} Å	r_{23-24} Å	r_{24-21} Å	r_{21-23} Å	r_{22-24} Å
MADMECl	3.04	2.83	3.05	2.82	4.23	4.07
Ni-MADMECl	2.70	2.67	2.74	2.70	3.83	3.81
Zn-MADMECl	2.89	2.84	2.91	2.86	4.05	4.08
Cu-MADMECl	2.82	2.78	2.84	2.81	3.97	3.98

Distortion of a structure of conjugated moieties are usually accompanied by changes in the ring currents and aromaticity of the π-electron system [44,45]. The most adequate method for assessing the aromaticity of π-conjugated systems is the NICS criterion (nuclear independent chemical shift) obtained from the data of quantum chemical calculations [46].
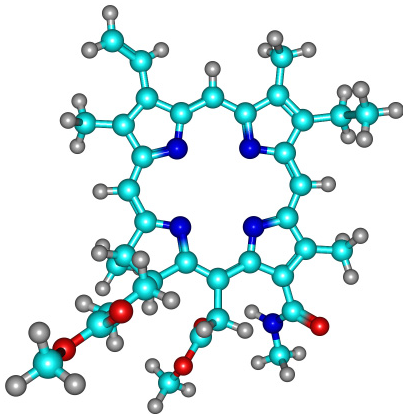
The following localization points were chosen for the NICS calculation: centers of "pockets" X1, X2, X3, and X4 (internal conjugation contour) and centers of five-membered rings A, B, C, and D (external conjugation contour) (Table 3). These data indicate that the formation of metal complexes leads to an increase in the aromaticity in both conjugation contours. An exception is the nuclear deshielding zone of a saturated five-member cycle D, which has an antiaromatic character [44] and, consequently, a positive NICS. In this case, the introduction of a metal ion is accompanied by a decrease in antiaromaticity. The effect of a metal on the aromaticity of the chlorine macrocycle is the most interesting. Thus, the aromaticity of the inner contour (X1, X2, X3, X4) decreases in the series Ni-MADMECl > Cu-MADMECl > Zn-MADMECl, which also corresponds to the degree of macroring acoplanarity (see above). At the same time, the aromaticity of the outer contour A, B, and C demonstrates an inverse relationship Zn-MADMECl > Cu-MADMECl > Ni-MADMECl (Table 3), as well as the antiaromaticity of the five-membered cycle D. Thus, it can be stated that a significant distortion of the planar structure of the chlorine macrocycle upon complex formation is also accompanied by a noticeable perturbation of the π-electron conjugation. This perturbation can result in energetic consequences, which were analyzed based on the energy data of the dianion calculated from the quantum chemical simulation of MADMECl and its metal complexes (see experimental section).

Table 3. NICS parameters (ppm).

	X_1	X_2	X_3	X_4	A	B	C	D
MADMECl	−12.13	−10.08	−10.53	−11.54	−0.60	−2.46	−3.25	+5.06
Zn-MADMECl	−14.35	−12.24	−11.95	−14.01	−6.31	−8.64	−8.35	+4.78
Cu-MADMECl	−15.76	−13.64	−13.13	−15.07	−5.65	−8.16	−8.24	+4.66
Ni-MADMECl	−16.72	−14.60	−13.67	−15.73	−4.58	−6.94	−7.37	+4.35

Table 4 data show that metalation of the macroligand leads to various consequences. Thus, the introduction of a zinc ion is accompanied by a decrease in the energy of the macroring, that is, its stabilization, apparently due to the preservation of the coplanarity of cyclic moieties (Table 1). At the same time, the decrease in the aromaticity of the inner contour leads to a compensatory increase in it in the five-membered cycles A, B, and C. Complexation with copper causes a slight increase in the dianion energy. At the same time, the formation of the nickel complex is accompanied by a noticeable increase in the energy of the macrocyclic core, apparently due to the strong acoplanarity of the latter (Table 1).

Table 4. Change in energy of the MADMECl dianion after complex formation.

	E (I) au	**$\Delta E = E(I) - E(I) \times$ kcal/mol**
2H	−2083.43 *	
Zn	−2083.35	−3.47
Cu	−2083.34	1.62
Ni	−2083.33	14.43

*—dianion MADMECl.

The data presented in Figure 1 indicate significant changes in the UV/Vis and CD spectra upon the formation of chlorin e6 13(N)-methylamide-15,17-dimethyl ester metal complexes. To quantify the experimental CD spectra, we calculated the molar coefficients of circular dichroism [37] $\Delta\varepsilon = \varepsilon_l - \varepsilon_r$, and as a measure of the chirality of macroheterocycles, the dissymmetry g-factor was determined via

$$g = \Delta\varepsilon / \varepsilon \qquad (1)$$

where ε is the molar extinction coefficient of the corresponding band in the UV/Vis spectrum.

The data presented in Table 5 show that the CD of both absorption bands (Soret and Q) follows the same regularities during the complexation of the chlorin e6 derivative. So, with the insertion of Zn, CD somewhat decreases, Ni and Cu increase significantly symbatic with the growth of acoplanarity (Tables 1 and 2) of the macroring and its distortion energy (Table 4). The dissymmetry g-factor, which is a measure of chirality, changes similarly. Therefore, it was possible to determine a clear relationship between the fundamental molecular properties of the chlorin e6 13(N)-methylamide-15,17-dimethyl ester metal complexes: acoplanarity—aromaticity—chirality.

Table 5. Spectral parameters of macroheterocycles in chloroform.

	λ, nm	Δε, l·mol⁻¹·cm⁻¹	ε, l·mol⁻¹·cm⁻¹	g-factor·10⁴
MADMECl	400	18.1	44697	4.05
	661	−4.2	15621	−2.67
Ni-MADMECl	417	91.2	68981	13.22
	636	−32.7	36574	−8.94
Cu-MADMECl	408	55.3	42931	12.87−6.59
	630	−15.3	23172	
Zn-MADMECl	416	6.3	26882	2.36
	636	−1.2	11294	−1.1

Taking into account the results obtained earlier [35], the influence of the central metal on the ability of the studied complexes to induce spiral liquid crystal phases is of undoubted interest. Therefore, in this work, solutions of MADMECl and its complexes were studied in a nematic mixture of alkoxycyanobiphenyls CB-2 (see experimental section). The appearance of fingerprint textures and Newton's rings in polarized light (Figure 2) unambiguously indicates the forming of a helical liquid crystal phase under the action of the introduced chiral dopants. Polarization microscopy was used to determine the clearance temperatures of the LC–chiral macroheterocycle systems, which are a measure of the thermal stability of the mesophase, at various concentrations of dopants.
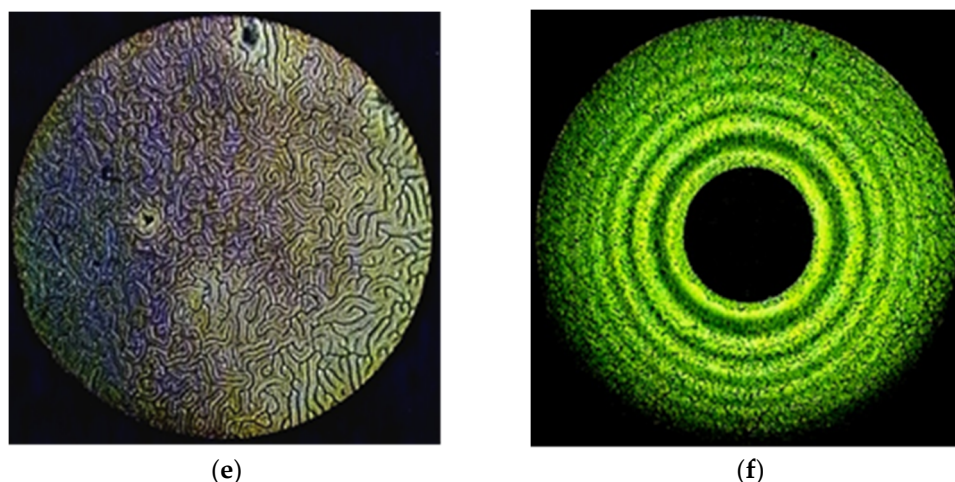

(a)

(b)

(c)

(d)

Figure 2. *Cont.*

(e)

(f)
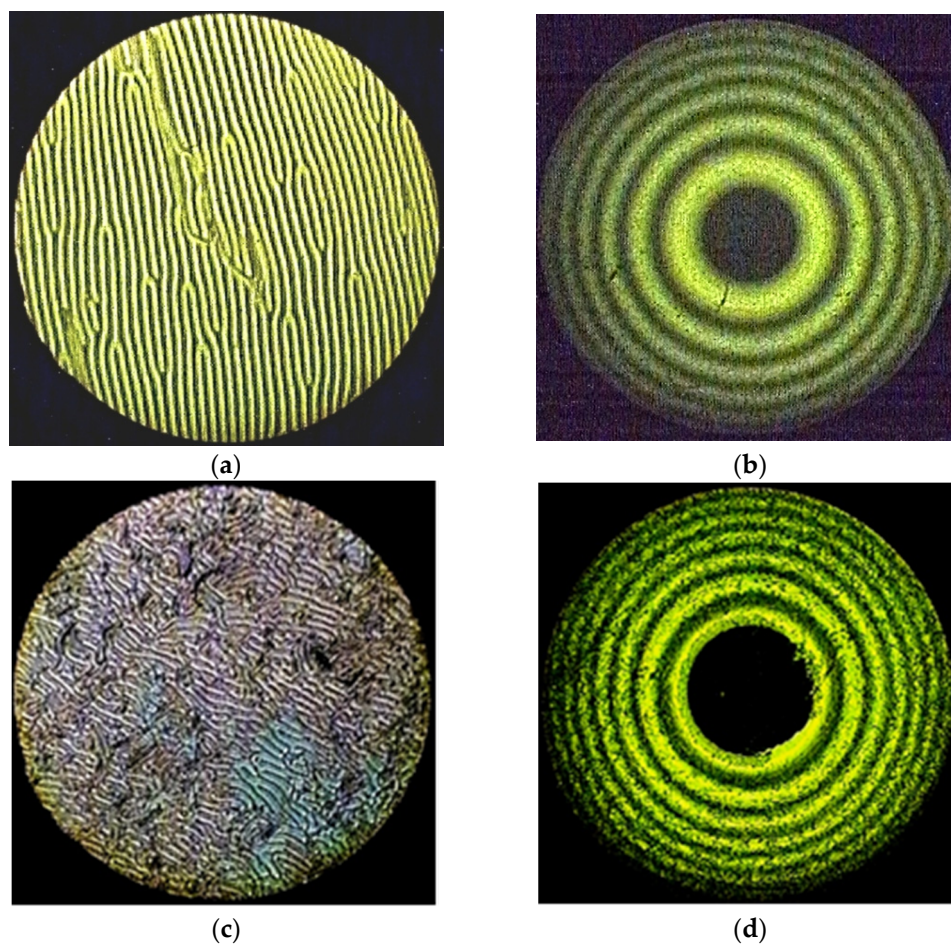
Figure 2. The "fingerprints" texture of the mixtures CB-2 with (**a**) 1.54% Ni-MADMECl; (**c**) 1.96% Cu-MADMECl; (**e**) 3.36% Zn-MADMECl at 70 °C. The system of Newton's rings of the same mixtures at 25 °C (wavelength of monochromatic light 551 nm) with (**b**) 1.54% Ni-MADMECl; (**d**) 1.96% Cu-MADMECl; (**f**) 3.36% Zn-MADMECl.

Figure 3 shows the concentration dependences of the relative clearance temperature (T_{NI}/T^o_{NI}, where T^o_{NI} is the transition temperature of the nematic–isotropic liquid without additive [47]). The slopes β of the $T_{NI}/T^o_{NI} = f(n_2)$ dependences are listed in Table 5, which quantitatively characterize the degree of dopant influence on the thermal stability of the mesophase. Based on the quantitative analysis of the Newton rings systems by the Grandjean–Cano method (see experimental section), the values of the helix pitch of chiral nematics were measured and the values of the helical twisting power (HTP) were calculated using the equation:

$$HTP = (p \cdot c \cdot r)^{-1} \tag{2}$$

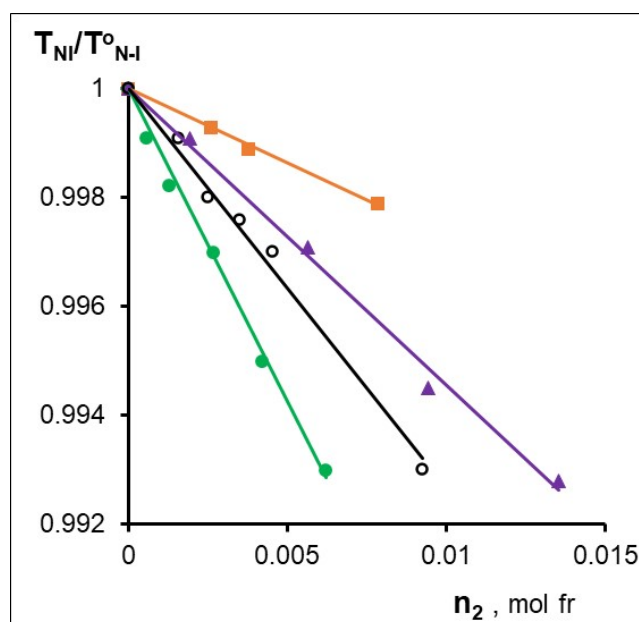where p is the pitch of the helix, c is the mole fraction of the dopant, and r is its enantiomeric purity.

Figure 3. Fragments of phase diagrams for the CB-2 mixtures with -○- MADMECl; -▲-Zn-MADMECl; -■-Cu-MADMECl; -●-Ni-MADMECl.

The concentration dependences of HTP are shown in Figure 4, and the maximum values of HTP are listed in the Table 6. The data presented in Figures 3 and 4 and in Table 6 indicate a strong influence of the metal in the MADMECl complexes on their behavior in the nematic liquid crystal. Thus, complexation can both increase and decrease the parameters given in Table 6. First of all, it draws attention to the anomalously high values of both β and HTP of the nickel complex of the chlorin e6 derivative. The reason for the significant HTP is the high optical activity associated with the highest acoplanarity of the complex, strong interactions with LC, and the contribution of supramolecular chirality [35].
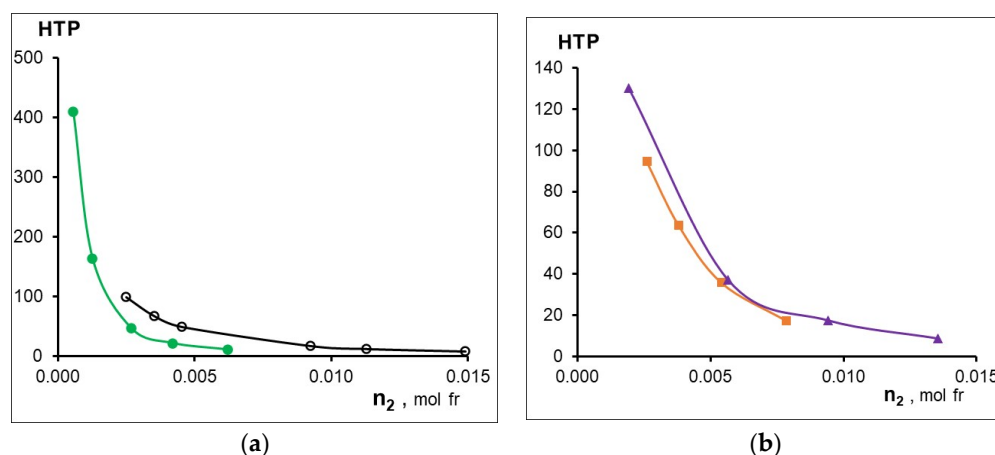

(a)   (b)

Figure 4. Effect of dopant concentration on its HTP (**a**) -○-MADMECl; -•- Ni-MADMECl; (**b**) -▲-Zn-MADMECl; -■-Cu-MADMECl.

Table 6. Effect of a metal on the thermal stability of the LC phase (β = d($T_{NI}/T°_{NI}$)/dn_2 and the maximum HTP.

Dopant	β, mol.fr.$^{-1}$	HTP$_{max}$, μM^{-1}
MADMECl	−0.73	97.9
Zn-MADMECl	−0.54	130.4
Cu-MADMECl.	−0.27	94.5
Ni-MADMECl	−1.15	409.2

However, a strong distortion of the planar structure of the macrocycle during the formation of Ni-MADMECl leads not only to the effective induction of the helical LC phase, but is also accompanied by a decrease in the ability of the dopant to efficiently incorporate the orientationally ordered LC structure [48]. Metal-less macrocycle MADMECl and its Zn complex, having the highest coplanarity and low optical activity (see above), nevertheless demonstrate a medium ability for chiral induction and close values of β. At the same time, a copper complex with medium acoplanarity and sufficiently high chirality slightly destabilizes the mesophase but does not show a high HTP (Table 6). Apparently, as in the case of Ni-MADMECl, the structure of dopant-LC solvates and the resulting supramolecular chirality can have a significant effect on the behavior of zinc and copper complex dopants in LCs. It should be noted that an increase in the content of all macrocyclic additives leads to a decrease in HTP due to the association of the latter, as previously shown [33].

3. Materials and Methods

3.1. Materials

Chlorin e6 13-(N)-methylamide-15,17-dimethyl ester (MADMECl) and its metal complexes (Zn-MADMECl, Cu-MADMECl, Ni-MADMECl) were studied. The synthesis and characterization of the compounds were carried out similarly to [35,49,50].

Chlorin e6 13-(N)-methylamide-15,17-dimethyl ester (MADMECl)

Methylamine, 6 mL of a 30 % aqueous solution, was added to a solution of 505 mg (0.833 mmol) of methyl pheophorbide a in 15 mL of dioxane. We obtained 492 mg (93%) of the title compound as a dark green powder:

1H NMR (500 MHz, CDCl3, 25 °C): δ 9.68 (s, 1H), 9.65 (s, 1H), 8.85 (s, 1H), 8.09 (dd, 3J = 8.07 Hz, 1H), 6.36 (dd, 3J = 11.87 Hz, 1H), 6.35 (bs, 1H), 6.34 (dd, 3J = 10.6 Hz, 1H), 5.54 (d, 2J = 18.87 Hz, 1H),　　　　5.28 (d, 2J = 19.07 Hz, 1H),　　　　4.51 (q, 3J = 4.51 Hz, 1H), 4.39 (dd, 3J = 4.38 Hz, 1H), 3.80 (s, 3H), 3.78 (m, 2H), 3.66 (s, 3H), 3.52 (s, 3H), 3.51 (s, 3H), 3.33 (s, 3H), 3.18 (d, 3J = 4.53 3H), 2.59 (m, 1H), 2.24 (m, 1H), 2.21 (m, 1H), 1.81 (m, 1H), 1.77 (d, 3J = 7.50 3H), 1.74 (t, 3J = 7.93 3H), −1.56 (bs, 1H), −1.78 (bs, 1H) ppm. 13C NMR (125 MHz, CDCl3, 25 °C): δ 174.25, 173.54, 170.11, 168.82, 166.67, 154.21, 149.08, 144.75, 138.91, 136.10, 134.96, 134.95, 134.81, 134.53, 130.17, 129.89, 129.46, 128.08, 121.62, 102.02, 101.42, 98.84, 93.67, 53.08, 52.07, 51.64, 49.29, 37.73, 31.12, 29.64, 27.20, 23.06, 19.68, 17.75, 12.19, 11.92, 11.35. ppm.

UV−vis (CHCl3) λmax: 406, 505, 610, 668 nm. Anal. Calcd. for C37N5H43O5 (637.33): C, 69,66%; H, 6.8%; N, 10.98%.; O, 12.56% Found: C, 69.8%; H, 6.6%; N, 11.05%; O, 12.5%.

Zn-Chlorin e6 13-(N-methylamide)-15,17-dimethyl ester. (Zn-MADMECl)

Zn-chlorin e6 13(1)-N-methylamid 15(2),17(3) dimethyl ester (Zn-MADMECl) was obtained from 103.8 mg of Chlorin e6 (13 (N)-methylamide-15,17-dimethyl ester (MADMECl) and 216.0 mg of zinc acetate. The yield of Zn-MADMECl was 80.9 mg (71%):

1H NMR (500 MHz, CDCl3, 25 °C): δ 9.40 (s, 1H), 9.35 (s, 1H), 8.60 (s, 1H), 7.96 (dd, 3J = 11.44 Hz, 1H), 6.08 (dd, 3J = 16.05 Hz, 1H), 6.12 (bs, 1H), 5.92 (dd, 3J = 5.9 Hz, 1H), 5.17 (d, 2J = 18.19 Hz, 1H), 4.85 (d, 2J = 19.07 Hz, 1H), 4.35 (q, 3J = 6.74 Hz, 1H), 4.16 (d, 3J = 8.74 Hz, 1H), 3.75 (s, 3H), 3.60 (q, 3J = 7.1 Hz 2H), 3.52 (s, 3H), 3.36 (s, 3H), 3.18 (m, 6H), 3.01 (s, 3H), 2.47 (m, 1H), 2.16 (m, 1H), 2.07 (m, 1H), 1.76 (m, 1H), 1.71 (d, 3J = 7.10 3H), 1.64 (t, 3J = 7.5 3H) ppm. 13C NMR (125 MHz, CDCl3, 25 °C): δ 174.67, 173.43, 171.4, 165.09, 161.56, 152.82, 147.55, 147.31, 145.06, 143.59, 141.42, 139.81, 138.28, 133.47, 132.78, 131.5, 130.28, 119.7, 102.97, 101.67, 100.91, 93.48, 52.38, 51.88, 51.54, 47.1, 37.7, 30.83, 29.05, 26.88, 22.89, 19.19, 17.53, 12.29, 11.9, 10.93 ppm. UV−vis (CHCl3) λmax: 300, 411, 516, 600, 641 nm. Anal. Calcd. for ZnC37N5H41O5 (699.24): Zn, 9.14%; C, 63,50%; H, 5.91%; N, 10.01%.; O, 11.44% Found: C, 63.41%; H, 5.65%; N, 10.21%; O, 11.32%.

Cu-Chlorin e6 13-(N-methylamide)-15,17-dimethyl ester. (Cu-MADMECl)

Cu-Chlorin e6 13-(N-methylamide)-15,17-dimethyl ester (Cu-MADMECl) was obtained from 93.1 mg Chlorin e6 (13 (N)-methylamide-15,17-dimethyl ester (MADMECl) and 357.1 mg copper acetate. The yield of Cu-MADMECl was 39.7 mg (67%):

UV−vis (CHCl3) λmax: 412.2, 600.6, 610, 641 nm. Anal. Calcd. for CuC37N5H41O5 (698.24): Cu, 9.01% C, 63,59%; H, 5.92%; N, 10.03%.; O, 11.45% Found: C, 63.9%; H, 5.6%; N, 10.2%; O, 11.1%.

Ni-Chlorin e6 13-(N-methylamide)-15,17-dimethyl ester. (Ni-MADMECl)

We added 217 mg (0.34 mmol) of chlorin e6 13(1)-N-methylamide 15(2),17(3)-dimethyl ether (MADMECl) and 340 mg (2.90 mmol) Ni(OAc)2 to a solution of 0.5 mL (4.87 mmol) of acetylacetone in 10 mL of toluene. We obtained 140 mg (59%) of the title compound (Ni-MADMECl) as a dark emerald green powder:

1H NMR (500 MHz, CDCl3, 25 °C): δ 9.11 (s, 1H), 9.04 (s, 1H), 8.06 (s, 1H), 7.81 (dd, 3J = 11.58 Hz, 1H), 6.04 (d, 3J = 17.61 Hz, 1H), 6.24 (bs, 1H), 5.94 (d, 3J = 11.49 Hz, 1H), 4.94 (d, 2J = 18.64 Hz, 1H), 4.52 (d, 2J = 19.21 Hz, 1H), 4.14 (q, 3J = 6.34 Hz, 1H), 3.98 (dd, 3J = 6.92 Hz, 1H), 3.84 (s, 3H), 3.66 (s, 3H), 3.57 (m, 2H), 3.2 (s, 3H), 3.19 (d, 3J = 4.90 3H), 3.15 (s, 3H), 3.14 (s, 3H), 2.45 (m, 1H), 2.35 (m, 1H), 1.78 (m, 1H), 1.61 (m, 1H), 1.58 (t, 3J = 7.59 3H), 1.49 (d, 3J = 7.09 3H) ppm. 13C NMR (125 MHz, CDCl3, 25 °C): δ 173.49, 173.33, 170.33, 156.03, 153.12, 145.46, 132.42, 141.83, 140.97, 139.93, 138.01, 137.79, 134.74, 133.46, 129.51, 141.27, 120.15, 100.29, 139.29, 133.84, 103.31, 101.2, 92.48, 52.03, 51.68, 47.37, 51.76, 31.08, 36.48, 26.99, 27.09, 19.25, 19.88, 17.35, 11.98, 11.86, 10.94. ppm. UV−vis (CHCl3)

λmax: 407.2, 508, 592, 639 nm Anal. Calcd. for $NiC_{37}N_5H_{41}O_5$ (693.246): Ni 8.36%; C, 64.05%; H, 5.96%; N, 10.09%; O, 11.54% Found: C, 64.8%; H, 5.7%; N, 10.3 %; O, 11.0%.

Liquid crystalline mixtures based on cyanobiphenyl derivatives (CB-2) were used to study chiral induction. The nematic mixture CB-2 is composed of two components: 55% 4-pentyloxy-4′-cyanobiphenyl (5OCB) and 45% 4-heptyloxy-4′-cyanobiphenyl (7OCB) (Qualification "Pure for analysis" Reahim). The phase transition temperatures of CB-2 are as follows: crystal → 22 °C → nematic → 74.5 °C → isotropic [51]. Liquid crystalline mixtures with dopants were prepared gravimetrically by mixing at temperatures corresponding to the isotropic liquid state. At all the temperatures of the study, separation of mixtures was not observed; it was recorded by the method of polarization microscopy.

3.2. Measurement of UV/Vis, CD Spectra

Circular dichroism (CD) spectra of MADMECl and its complexes solutions were recorded on a «Jasco 1500» spectrometer. UV/Vis spectra were obtained on a Perkin Elmer «Lambda 20» scanning spectrophotometer. The molar extinction coefficients (ε and $\Delta\varepsilon = \varepsilon_l - \varepsilon_r$) were calculated using the Beer–Lambert equation.

3.3. NMR Measurement

^{1}H, ^{13}C NMR, HMBC [15]N-^{1}H spectra were recorded on "Avance III Bruker 500" NMR spectrometer with operating frequencies of 500.17, 125.77 MHz, and 50.68 MHz, respectively. A 5 mm 1H/31P/D-BBz-GRD Triple Resonance Broad Band Probe (TBI) was employed.

3.4. Quantum chemical Calculations

M-MADMECl structures were optimized by using the CAM-B3LYP functional of the Gaussian 09W [52] software package with base sets of 6–31 G (d,p) (the optimized Cartesian coordinates of MADMECl and its complexes with Zn, Cu, and Ni are available in the Supplementary Materials). TD-DFT calculations were then carried out using the CAM-B3LYP/6–31 G(d,p) scrf = (cpcm, solvent = chloroform) functional since it contains a long-range correction. The number of excited states was 25.

NMR shielding constants were calculated using the GIAO method [53] with basis CAM-B3LYP/6-311++(d,p) scrf = (cpcm, solvent = chloroform). According to recommendations [54,55], benzene and TMS were chosen as standards for calculating the chemical changes of sp2- and sp3-hybridized carbons, respectively. The reference compounds geometry and shielding parameters were calculated at the same theory level as the studied compounds. The chemical shifts δ_i of the M-MADMECl were calculated according to the equation:

$$\delta_i = \sigma_{ref} - \sigma_i + \delta_{ref} \tag{3}$$

where σ_{ref} and σ_i are the shielding constants calculated for MADMECl and standards, δ_{ref} is an experimental chemical shift of the reference compound (128.5 ppm for benzene ^{13}C NMR, 0 ppm for TMS). Calculations of the nucleus-independent chemical shift (NICS) [56] were performed for the M-MADMECl structures.

Chemcraft software [57] was applied for the preparation of input data files, as well as for processing and visualization of the computed results.

3.5. Measurement of Phase Transitions Temperatures

The study of the mesomorphic properties was carried out by polarization microscopy on a «Polam P211» polarizing microscope equipped with a thermotable. The phase transition temperatures were measured with an accuracy of ±0.1 °C. To obtain textures, a cell of two plane-parallel glasses was used without special surface treatment.

3.6. Measurement of Pitch

The helical pitch of the chiral phases at various temperatures and dopant concentrations was measured by the Grandjean–Cano method [58] using a convex lens and a plane-parallel plate at a monochromatic light wavelength of 551 nm. For the

CB-2 + MADMECl system, the helix pitch was directly measured from the "fingerprint" textures obtained with a camera-mounted microscope [59,60]. The pitch values measured by the two methods coincided within the limits of the experimental error. The ability to form a spiral mesophase was described by the helical twisting power (HTP) according to Equation (2). The error in determining HTP was $\pm 1 \ \mu m^{-1}$.

4. Conclusions

The effect of the nature of a central metal on the geometry, aromaticity, chirality, and ability to twist the nematic phase of macroheterocyclic complexes based on modified natural chlorin e6 was studied. Quantum chemical optimization of geometry of chlorin e6 13(N)-methylamide-15,17-dimethyl ester (MADMECl) and its Zn, Cu, and Ni complexes was carried out using the DFT (CAM-B3LYP/6–31 G(d,p) functional) method. The adequacy of the simulation was established by comparing the calculated and experimental UV/Vis, CD, ^{1}H, and ^{13}C NMR spectra. To assess the degree of acoplanarity, we measured the deviation of macrocyclic ligand atoms from the plane of intracyclic nitrogen atoms and the distortion energy of the macrocyclic dianion. The degree of acoplanarity of the macroring as a result of complex formation was shown to be located in the series Ni-MADMECl > Cu-MADMECl > Zn-MADMECl. Aromaticity was evaluated using the NICS criterion (nuclear independent chemical shift). An increase in the degree of aromaticity of the macrocycle upon complex formation was established. At the same time, the aromaticity of the inner conjugation contour corresponds to the series Ni-MADMECl > Cu-MADMECl > Zn-MADMECl, while the outer conjugation contour, which includes three five-membered pyrrolenine rings, is characterized by the reverse degree of aromaticity. The circular dichroism of the Soret and the Q-bands was experimentally evaluated, indicating an increase in CD with an increase in the degree of acoplanarity and aromaticity of the inner contour of the conjugation. The g-factor of dissymmetry changes in a similar way. The induction of helical phases was studied using polarization microscopy in mixtures of LCs based on cyanobiphenyls and MADMECl macrocyclic metal complexes. The clearance temperatures and the helix pitch of the mesophases were measured. A strong influence of the metal on the phase transition temperature and helical twisting power was found.

Author Contributions: Conceptualization, V.B. and O.I.K.; methodology, V.A.; validation, V.B., V.A.; formal analysis, V.A.; investigation, V.A., I.N., A.B., D.B., O.S.; project administration, O.I.K.; funding acquisition, O.I.K. All authors have read and agreed to the published version of the manuscript.

Conflicts of Interest: The authors declare no conflict of interest.

References

1. Kadish, K.M.; Smith, K.M.; Guilard, R. Handbook of Porphyrin Science with Applications to Chemistry, Physics, Materials Science, Engineering, Biology and Medicine. In *Physicochemical Characterization*; World Scientific Publishing Co. Pte. Ltd.: Singapore, 2010; Volume 7.

2. Lucky, S.S.; Soo, K.C.; Zhang, Y. Nanoparticles in Photodynamic Therapy. *Chem. Rev.* **2015**, *115*, 1990–2042. [CrossRef] [PubMed]

3. Le Guern, F.; Ouk, T.-S.; Yerzhan, I.; Nurlykyz, Y.; Arnoux, P.; Frochot, C.; Leroy-Lhez, S.; Sol, V. Photophysical and Bactericidal Properties of Pyridinium and Imidazolium Porphyrins for Photodynamic Antimicrobial Chemotherapy. *Molecules* **2021**, *26*, 1122. [CrossRef] [PubMed]

4. Gürses, A.; Açıkyıldız, M.; Güneş, K.; Gürses, M.S. *Dyes and Pigments*; Springer: Berlin/Heidelberg, Germany, 2016. [CrossRef]

5. Sorokin, A.B. Phthalocyanine Metal Complexes in Catalysis. *Chem. Rev.* **2013**, *113*, 8152–8191. [CrossRef]

6. Koifman, O.I.; Ageeva, T.A.; Beletskaya, I.P.; Averin, A.D.; Yakushev, A.A.; Tomilova, L.G.; Dubinina, T.V.; Tsivadze, A.Y.; Gorbunova, Y.G.; Martynov, A.G.; et al. Macroheterocyclic Compounds—A Key Building Block in New Functional Materials and Molecular Devices. *Macroheterocycles* **2020**, *13*, 311–467. [CrossRef]

7. Peters, M.K.; Herges, R. Insertion of Ni(I) into Porphyrins at Room Temperature: Preparation of Ni(II)porphyrins, and Ni(II)chlorins and Observation of Hydroporphyrin Intermediates. *Inorg. Chem.* **2018**, *57*, 3177–3182. [CrossRef]

8. Colombo, A.; Di Carlo, G.; Dragonetti, C.; Magni, M.; Orbelli Biroli, A.; Pizzotti, M.; Roberto, D.; Tessore, F.; Benazzi, E.; Bignozzi, C.A.; et al. Coupling of Zinc Porphyrin Dyes and Copper Electrolytes: A Springboard for Novel Sustainable Dye-Sensitized Solar Cells. *Inorg. Chem.* **2017**, *56*, 14189–14197. [CrossRef]

9. Tessore, F.; Di Carlo, G.; Forni, A.; Righetto, S.; Limosani, F.; Orbelli Biroli, A. Second Order Nonlinear Optical Properties of 4-Styrylpyridines Axially Coordinated to A4 ZnII Porphyrins: A Comparative Experimental and Theoretical Investigation. *Inorganics* **2020**, *8*, 45. [CrossRef]

10. Dommaschk, M.; Thoms, V.; Schütt, C.; Näther, C.; Puttreddy, R.; Rissanen, K.; Herges, R. Coordination-Induced Spin-State Switching with Nickel Chlorin and Nickel Isobacteriochlorin. *Inorg. Chem.* **2015**, *54*, 9390–9392. [CrossRef] [PubMed]

11. Lu, H.; Kobayashi, N. Optically Active Porphyrin and Phthalocyanine Systems. *Chem. Rev.* **2016**, *116*, 6184–6261. [CrossRef]

12. Kelly, S.M.; O'Neill, M. Liquid Crystals for Electro-Optic Applications. In *Handbook of Advanced Electronic and Photonic Materials and Devices*; Academic Press: Cambridge, UK, 2000; Volume 7, pp. 1–66.

13. Bisoyi, H.K.; Li, Q. Light-Driven Liquid Crystalline Materials: From Photo-Induced Phase Transitions and Property Modulations to Applications. *Chem. Rev.* **2016**, *116*, 15089–15166. [CrossRef]

14. Li, Q.; Green, L.; Venkataraman, N.; Shiyanovskaya, I.; Khan, A.; Urbas, A.; Doane, J.W. Reversible Photoswitchable Axially Chiral Dopants with High Helical Twisting Power. *J. Am. Chem. Soc.* **2007**, *129*, 12908–12909. [CrossRef] [PubMed]

15. Ma, J.; Xuan, L. Towards nanoscale molecular switch-based liquid crystal displays. *Displays* **2013**, *34*, 293–300. [CrossRef]

16. Onuchak, L.A.; Arutunov, J.I.; Kuraeva, J.G. Method for Analysis of Structural and Optical Isomers. Russian Patent RU 2528126, 10 September 2014.

17. Matt, B.; Pondman, K.M.; Asshoff, S.J.; ten Haken, B.; Fleury, B.; Katsonis, N. Soft Magnets from the Self-Organization of Magnetic Nanoparticles in Twisted Liquid Crystals. *Angew. Chem. Int. Ed.* **2014**, *53*, 12446–12450. [CrossRef]

18. Eelkema, R. Photo-responsive doped cholesteric liquid crystals. *Liq. Cryst.* **2011**, *38*, 1641–1652. [CrossRef]

19. Van Delden, R.A.; Schoevaars, A.M.; Feringa, B.L. A Novel Donor Acceptor Substituted Chiroptical Molecular Switch: Physical Properties and Photoisomerization Behavior. *Mol. Cryst. Liq. Cryst.* **2000**, *344*, 1–6. [CrossRef]

20. Feringa, B.L.; van Delden, R.A.; Koumura, N.; Geertsema, E.M. Chiroptical Molecular Switches. *Chem. Rev.* **2000**, *100*, 1789–1816. [CrossRef]

21. Wang, Y.; Li, Q. Light-Driven Chiral Molecular Switches or Motors in Liquid Crystal Media, Liquid Crystals Beyond Displays: Chemistry. In *Physics. and Applications*; Quan, L., Ed.; John Wiley & Sons. Inc.: Hoboken, NJ, USA, 2012; pp. 213–249.

22. Popov, P.; Honaker, L.W.; Mirheydari, M.; Mann, E.K.; Jakli, A. Chiral nematic liquid crystal microlenses. *Sci. Rep.* **2017**, *7*, 1603. [CrossRef]

23. Cachelin, P.; Green, J.P.; Peijs, T.; Heeney, M.; Bastiaansen, W.M. Optical Acetone Vapor Sensors Based on Chiral Nematic Liquid Crystals and Reactive Chiral Dopants. *Adv. Opt. Mater.* **2016**, *4*, 592–596. [CrossRef]

24. Van Delden, R.A.; Koumura, N.; Harada, N.; Feringa, B.L. Unidirectional rotary motion in a liquid crystalline environment: Color tuning by a molecular motor. *PNAS* **2002**, *99*, 4945–4949. [CrossRef]

25. Eelkema, R.; Pollard, M.M.; Katsonis, N.; Vicario, J.; Broer, D.J.; Feringa, B.L. Rotational Reorganization of Doped Cholesteric Liquid Crystalline Films. *J. Am. Chem. Soc.* **2006**, *128*, 14397–14407. [CrossRef]

26. Eelkema, R. Liquid Crystals as Amplifiers of Molecular Chirality. Ph.D. ThesIs, University of Groningen, Groningen, The Netherlands, 2006.

27. Watanabe, G.; Yoshida, J. Molecular Dynamics Approach for Predicting Helical Twisting Powers of Metal Complex Dopants in Nematic Solvents. *J. Phys. Chem. B* **2016**, *120*, 6858–6864. [CrossRef]

28. Yoshida, J.; Watanabe, G.; Kakizawa, K.; Kawabata, Y.; Yuge, H. Tris(β-diketonato) Ru(III) Complexes as Chiral Dopants for Nematic Liquid Crystals: The Effect of the Molecular Structure on the Helical Twisting Power. *Inorg. Chem.* **2013**, *52*, 11042–11050. [CrossRef]

29. Engelmann, M.; Braun, M.; Kuball, H.-G. Helical twisting power of chiral titanium complexes in nematic compounds. *Liq. Cryst.* **2007**, *34*, 73–77. [CrossRef]

30. Braun, M.; Hahn, A.; Engelmann, M.; Fleischer, R.; Frank, W.; Kryschi, C.; Haremza, S.; Krschner, K.; Parker, R. Bis-Chelated Imine-Alkoxytitanium Complexes: Novel Chiral Dopants with High Helical Twisting Power in Liquid Crystals. *Chem. Eur.J.* **2005**, *11*, 3405–3412. [CrossRef] [PubMed]

31. Ivashchenko, A.V. *Dichroic Dyes for Liquid Crystal Displays*; CRC Press Taylor & Francis Group: Boca Raton, FL, USA, 1994.

32. Burmistrov, V.A.; Novikov, I.V.; Aleksandriiskii, V.V.; Semeikin, A.S.; Koifman, O.I. Favourable combination of axial coordination and inclusion for effective chiral transfer from metal porphyrin to nematic liquid crystals. *Liq. Cryst.* **2021**, *48*, 794–805. [CrossRef]

33. Popov, N.; Honaker, L.W.; Popova, M.; Usol'tseva, N.; Mann, E.K.; Jákli, A.; Popov, P. Thermotropic liquid crystal—Assisted chemical and biological sensors. *Materials* **2018**, *11*, 20. [CrossRef] [PubMed]

34. Zahn, S.; Proni, G.; Spada, G.P.; Canary, J.W. Supramolecular detection of metal ion binding: Ligand conformational control of cholesteric induction in nematic liquid crystalline phases. *Chemistry* **2001**, *7*, 88–93. [CrossRef]

35. Burmistrov, V.A.; Novikov, I.V.; Aleksandriiskii, V.V.; Belykh, D.V.; Startseva, O.M.; Koifman, O.I. Chirality transfer from chlorin e6 13(N)-methylamide-15,17-dimethyl ester and its nickel complex to nematic liquid crystals. *J. Mol. Liq.* **2022**, *347*, 118330. [CrossRef]

36. Eelkema, R.; Feringa, B.L. Amplification of chirality in liquid crystals. *Org. Biomol. Chem.* **2006**, *4*, 3729–3745. [CrossRef] [PubMed]

37. Berova, N.; Di Bari, L.; Pescitelli, G. Application of electronic circular dichroism in configurational and conformational analysis of organic compounds. *Chem. Soc. Rev.* **2007**, *36*, 914. [CrossRef]

38. Nagano, Y.; Ogasawara, S.; Tamiaki, H. Regioisomeric synthesis of chlorin-e6 dimethyl esters and their optical properties. *J. Porphyr. Phthalocyanines.* **2018**, *22*, 1–8. [CrossRef]

39. Taniguchi, M.; Lindsey, J.S. Synthetic Chlorins, Possible Surrogates for Chlorophylls, Prepared by Derivatization of Porphyrins. *Chem. Rev.* **2017**, *117*, 344–535. [CrossRef]

40. Chaudhri, N.; Grover, N.; Sankar, M. Selective Conversion of Planar trans-Chlorins into Highly Twisted Doubly Fused Porphyrins or Chlorins via Oxidative Fusion. *Inorg. Chem.* **2018**, *57*, 6658–6668. [CrossRef] [PubMed]

41. Saha, B.; Ikbal, S.A.; Rath, S.P. Complexation of Chiral Zinc(II)Porphyrin Tweezer with Chiral Guests:Control, Discrimination and Rationalization of Supramolecular Chirality. *Inorg. Chem.* **2020**, *59*, 7795–7809. [CrossRef] [PubMed]

42. Ishizuka, T.; Grover, N.; Kingsbury, C.J.; Kotani, H.; Senge, M.O.; Kojima, T. Nonplanar porphyrins: Synthesis, properties, and unique functionalities. *Chem. Soc. Rev.* **2022**, *51*, 7560–7630. [CrossRef]

43. Shelnutt, J.A.; Song, X.-Z.; Ma, J.-G.; Jia, S.-L.; Jentzen, W.; Medforth, C.J. Nonplanar porphyrins and their significance in proteins. *Chem. Soc. Rev.* **1998**, *27*, 31–41. [CrossRef]

44. Krygowski, T.M.; Cyran´ski, M.K. Structural Aspects of Aromaticity. *Chem. Rev.* **2001**, *101*, 1385–1419. [CrossRef]

45. Chaudhri, N.; Grover, N.; Sankar, M. Nickel-Induced Skeletal Rearrangement of Free Base trans-Chlorins into Monofused NiII-Porphyrins: Synthesis, Structural, Spectral, and Electrochemical Redox Properties. *Inorg. Chem.* **2018**, *57*, 11349–11360. [CrossRef]

46. Chen, Z.; Wannere, C.S.; Corminboeuf, C.; Puchta, R.; von Rague´ Schleyer, P. Nucleus-Independent Chemical Shifts (NICS) as an Aromaticity Criterion. *Chem. Rev.* **2005**, *105*, 3842–3888. [CrossRef]

47. Burmistrov, V.A.; Alexandriysky, V.V.; Koifman, O.I. Influence of the molecular structure of a nematic solvent on hydrogen bonding with non-mesomorphic proton donors. *Liq. Cryst.* **1995**, *18*, 657–664. [CrossRef]

48. Dierking, I. Chiral liquid crystals: Structures, phases, effects. *Symmetry* **2014**, *6*, 444–472. [CrossRef]

49. Belykh, D.V.; Tarabukina, I.S.; Matveev, Y.S.; Kuchin, A.V. Nickel Complexes of Chlorophyll Derivatives. *Russ. J. Gen. Chem.* **2007**, *77*, 1300–1307. [CrossRef]

50. Tarabukina, I.S.; Pylina, Y.I.; Velegzhaninov, I.O.; Startceva, O.M.; Shadrin, D.M.; Belykh, D.V. Synthesis and cytotoxic activity of novel transition metal porphyrinates based on chlorophyll a derivatives. *Butl. Commun.* **2015**, *43*, 18–23, ROI: Jbc-01/15-43-7-18.

51. Aleksandriiskii, V.V.; Novikov, I.V.; Burmistrov, V.A. The dielectric properties of 4-pentyloxy-and 4-heptyloxy-4´-cyanobiphenyls and their eutectic mixture. *Russ. J. Phys. Chem.* **2003**, *77*, 1813–1816.

52. Frisch, M.J.; Trucks, G.W.; Schlegel, H.B.; Scuseria, G.E.; Robb, M.A.; Cheeseman, J.R.; Scalmani, G.; Barone, V.; Mennucci, B.; Petersson, G.A.; et al. *Gaussian 09, Rev. A.1*; Gaussian Inc.: Wallingford, CT, USA, 2009.

53. Ditchfield, R. Self-consistent perturbation theory of diamagnetism I. A gauge-invariant LCAO method for N.M.R. chemical shifts. *Mol. Phys.* **1974**, *27*, 789–807. [CrossRef]

54. Lodewyk, M.W.; Siebert, M.R.; Tantillo, D.J. Computational Prediction of 1H and 13C Chemical Shifts: A Useful Tool for Natural Product, Mechanistic, and Synthetic Organic Chemistry. *Chem. Rev.* **2012**, *112*, 1839–1862. [CrossRef] [PubMed]

55. Sarotti, A.M.; Pellegrinet, S.C. A Multi-standard Approach for GIAO 13C NMR Calculations. *J. Org. Chem.* **2009**, *74*, 7254–7260. [CrossRef]

56. De Proft, F.; Geerlings, P. Conceptual and Computational DFT in the Study of Aromaticity. *Chem. Rev.* **2001**, *101*, 1451–1464. [CrossRef] [PubMed]

57. Zhurko, G.A.; Zhurko, D.A. Available online:. http://www.chemcraftprog.com/index.html (accessed on 22 May 2020).

58. Nemati, A.; Shadpour, S.; Querciagrossa, L.; Mori, T.; Zannoni, C.; Hegmann, T. Highly Sensitive Tunable Chirality Amplification through Space Visualize for Gold Nanorods Capped with Axially Chiral Binaphthyl Derivatives. *ACS Nano.* **2019**, *13*, 1310312–1310326. [CrossRef]

59. Fukuda, K.; Suzuki, H.; Ni, J.; Tokita, M.; Watanabe, J. Relationship between Chemical Structure and Helical Twisting Power in Optically Active Imine Dopants Derived from (R)-(+)-1-(1-Naphthyl)ethylamine. *Jpn. J. Appl. Phys.* **2007**, *46*, 5208–5212. [CrossRef]
60. Pieraccini, S.; Ferrarini, A.; Spada, G.P. Chiral doping of nematic phases and its application to the determination of absolute configuration. *Chirality* **2008**, *20*, 749–759. [CrossRef] [PubMed]